Targeting Accuracy of Transcranial Power Cavitation Imaging for Blood-Brain Barrier Opening Using a Theranostic Phased Array

Alec Batts
Biomedical Engineering
Columbia University
New York, NY, USA
ajb2305@columbia.edu

Elisa Konofagou
Biomedical Engineering
Radiology
Columbia University
New York, NY, USA
ek2191@columbia.edu

***Abstract*— Transcranial ultrasound-based monitoring of focused ultrasound (FUS)-mediated blood-brain barrier (BBB) opening is a challenge due to signal attenuation, phase aberration and focal distortion resulting from acoustic wave propagation through the skull. However, transcranial passive cavitation mapping is critical for ensuring noninvasive, safe, and consistent treatment. Power cavitation imaging using a diagnostic phased array synchronized with a FUS-induced BBB opening protocol poses one solution for transcranial cavitation mapping given the minimal focal shift resulting from transcranial ultrasound transmission. 1.94 mm and 1.01 mm average axial and lateral focal shifts, respectively, through primate skulls were observed during *in vitro* experiments and were recapitulated consistently by simulations. Average axial and lateral shifts in the apparent location of a microbubble flow channel detected via transcranial power cavitation imaging of 1.13 mm and 0.50 mm, respectively, agreed well with simulation results and results of other studies demonstrating registration errors after transcranial imaging of a microbubble flow channel.**

Keywords—blood-brain barrier opening, cavitation mapping, theranostic, transcranial imaging, focused ultrasound

I. Introduction

Focused ultrasound (FUS)-induced blood-brain barrier (BBB) opening in conjunction with systemically administered microbubbles (MBs) is a safe, noninvasive and reversible technique for delivering therapeutics to the brain. Previous work has demonstrated correlation between the acoustic pressure applied during FUS transmission and the type and extent of cavitation activity [1], [2], prompting development of ultrasound-based cavitation detection and monitoring techniques for use during the BBB opening procedure. Cavitation detection is typically achieved through the use of a single element passive cavitation detector (PCD) [3], [4], which may distinguish between stable and transient cavitation in addition to inferring cavitation dose, but fails to provide spatial information. Cavitation mapping techniques employing a diagnostic ultrasound linear or phased array address the spatial limitation of PCD by utilizing beamforming techniques to map cavitation events to their spatial points of origin [5], [6]. While cavitation mapping techniques have shown promise in preclinical mouse models, one of the major barriers to clinical translation is the highly attenuating and heterogeneously structured human skull. Phase aberration, signal attenuation and beam distortion caused by the irregular trabecular structure of the skull makes traditional ultrasound imaging and monitoring techniques challenging [7]. This study builds on previous work demonstrating the use of a passive cavitation technique called power cavitation imaging to guide FUS-induced BBB opening in mice [8]. Herein, we demonstrate the feasibility and evaluate the targeting accuracy of a single diagnostic phased array operated at a frequency of 1.5 MHz to perform transcranial power cavitation imaging synchronized with a BBB opening FUS protocol and to map cavitation activity through primate skulls.

This study was supported in part by NIH R01AG038961 and R01EB009041.

II. Materials and Methods

A. Pressure Calibration and in vitro Focal Shift Detection

A diagnostic phased array (P4-1, ATL, Philips) with a center frequency of 2.5 MHz (Bandwidth: 1.5 MHz – 3.5 MHz, 96 elements), was operated at 1.5 MHz for transcranial imaging by a research ultrasound system (Vantage 256, Verasonics Inc.). The P4-1, focused at ~35 mm was submerged in a degassed water bath beneath a fragment of non-human primate (NHP) or human skull parietal skull bone with average thicknesses of 2.25 and 4.65 mm, respectively. A needle hydrophone (HNP-0200, Onda Corporation), affixed to a three-axis positioning system was translated in raster scan mode to map the pressure at the

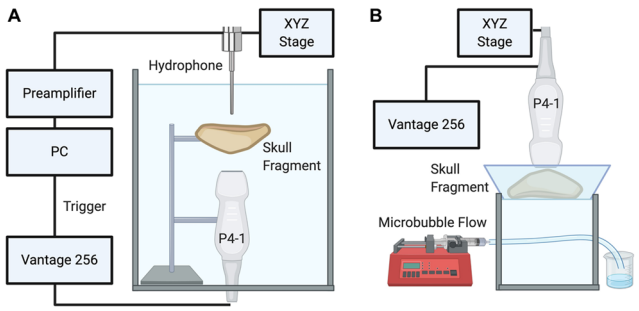

Fig. 1: *In vitro* experimental setup for (A) hydrophone focal mapping experiments and (B) power cavitation imaging experiments.

focus in free-field, and through both primate skull models (Fig. 1A).

B. Flow Channel Experimental Setup

The P4-1, affixed to the three-axis positioning system was placed 3-5 mm above a primate skull fragment submerged in a degassed water bath (Fig. 1B). The water bath containing the skull fragment was placed above a 254 µm diameter flow channel submerged in a degassed water tank at a depth of ~35 mm from the transducer face. In-house manufactured, polydisperse, lipid-shelled microbubbles at a concentration of 8.0E8 MBs/mL were continuously flowed through the channel at a velocity of 2.3 – 8.9 mm/s by a syringe pump (Genie Plus, Kent Scientific). B-mode imaging of the flow channel without the skull in place was used to establish reference coordinates for the location of the flow channel, while transcranial power cavitation imaging was performed in the manner described below.

C. Power Cavitation Imaging

The P4-1 focused transmit/receive sequences were synchronized via a custom MATLAB script to transmit ~3 cycle pulses at 450 kPa and receive 500 frames of passive cavitation images acquired at a rate of 1000 Hz to form a single power cavitation image of the flow channel. Each set of radiofrequency (RF) data was reconstructed using delay and sum (DAS) beamforming based on absolute time delays. 12-20 power cavitation images acquired at a rate of approximately 0.5 Hz were spatiotemporally filtered using a singular value decomposition (SVD) clutter filter to isolate flow, and averaged to form a final power cavitation image. Eigenvalue cutoff values for SVD filtering were selected during post-processing depending on the thickness and structural irregularity of the skull fragment.

D. Simulation Parameters

The k-Wave MATLAB toolbox was used to reconstruct the P4-1 phased array in 3D on a computational grid with a resolution of 8 points/wavelength. The resulting pressure distribution from a transcranial 3-cycle pulse at a frequency of 1.5 MHz and 1.0 MPa input peak negative pressure (PNP) was recorded in 3D. Density, sound speed, and absorption maps were derived from micro-CT scans of primate skull bone fragments of 80 µm isotropic resolution (MI Labs 3D optical CT scanner). In order to simulate received backscattered signal from the microbubble flow channel, a 254 µm diameter circular source was positioned at a depth of 38 mm from the simulated P4-1 phased array in 2D, emitting simulated echoes at the array frequency of 1.5 MHz. Single-frame RF data was beamformed using an analogous DAS beamforming procedure to that of PCI post-processing described above.

III. Results

A. Transmit Transcranial Focal Shift

In order to determine the predicted focal shift upon transmission through NHP and human skulls using the theranostic array configuration, the focal shift was detected with a hydrophone and compared to *in silico* results. In both *in vitro* experiments and simulations, the P4-1 was focused at approximately 35 mm. The hydrophone detected axial and

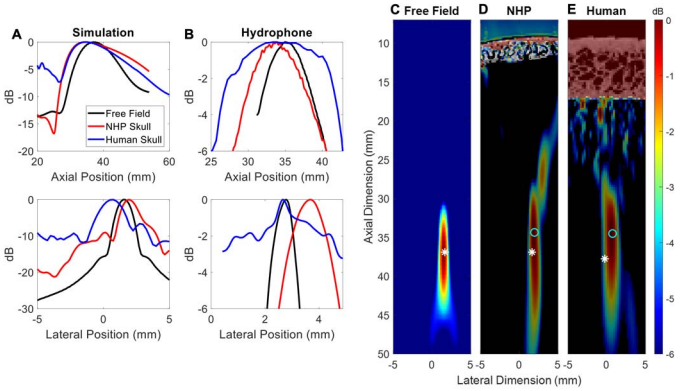

Fig. 2: Focal shift after transcranial FUS transmission. Axial and lateral focus profiles determined (A) *in silico* and (B) *in vitro*. Simulated beam focus profiles in (C) free field and after transcranial transmission through (D) the NHP skull and (E) the human skull. Position of the focus in free field and after skull transmission indicated by white asterisk and cyan circle, respectively.

lateral focal shifts through the NHP skull of 1.17 mm and 0.90 mm, respectively, and axial and lateral focal shifts through the human skull of 1.63 mm and 0.12 mm, respectively (Fig. 2B). Simulations revealed axial and lateral focal shifts through the NHP skull of 2.55 mm and 2.10 mm, respectively, and axial and lateral focal shifts through the human skull of 2.40 mm and 0.90 mm, respectively (Fig. 2A, C-E). While there was an average discrepancy in simulated axial and lateral focal shift for both primate skull models of 1.1 mm and 0.99 mm respectively, when compared to hydrophone measurements, the simulated focal position based on a focal depth of 35 mm agreed well with in vitro hydrophone-measured focal position within 2.3 – 9.2 percent error. Given these results, the P4-1 focused transmit at 1.5 MHz was expected to yield, on average, a 1.94 mm axial shift and 1.01 mm lateral shift upon transmission through primate skulls.

B. Transcranial Power Cavitation Imaging

In order to determine the feasibility of the theranostic array configuration to accurately map cavitation activity beneath primate skulls at safe acoustic pressures for BBB opening, transcranial PCI was used to image a 254 µm diameter channel in cross-section with flowing MBs and was compared to B-mode images in the absence of skull bone. PCI were spatiotemporally filtered using an SVD filter with eigenvalue cutoffs dependent on skull thickness and structural complexity. PCI revealed axial and lateral shifts in the location of the flow channel beneath the NHP skull of 1.50 and 0.90 mm, respectively (Fig. 3A) and axial and lateral shifts of the channel beneath the human skull of 1.20 and 0.30 mm, respectively (Fig. 3B), compared to B-mode reference coordinates in free-field. Furthermore, PCI through the NHP skull required an average eigenvalue cutoff of 5 to minimize skull signal, while an average eigenvalue cutoff of 10 was required to reduce signal intensity of the human skull. While modifying the eigenvalue cutoff values improved visibility of the flow channel, neither the cutoff value nor flow velocity affected the observed flow channel shift. Single-frame DAS beamformed images of the flow channel through both skull models were used to validate the flow channel shift observed with PCI. Simulations revealed axial and lateral shifts in the location of

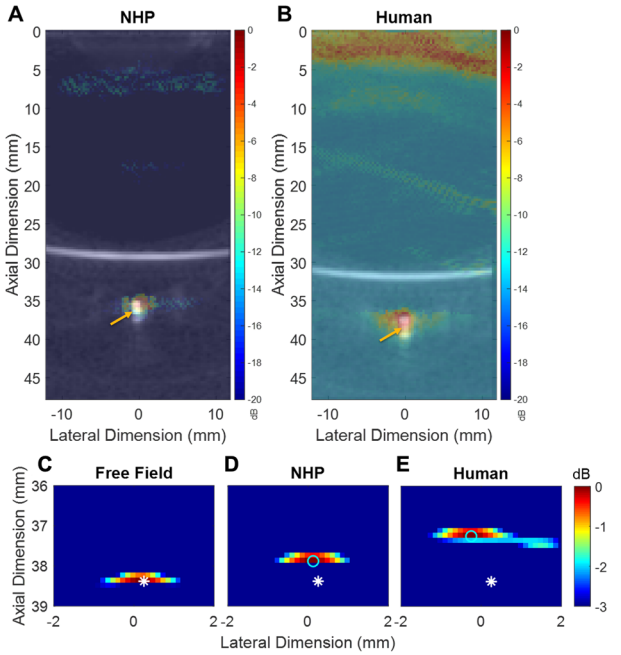

Fig. 3: Transcranial power cavitation imaging. Power cavitation images with B-mode overlay (center of flow channel indicated by yellow arrow) through (A) NHP skull with eigenvalue cutoff of 5 and (B) human skull with eigenvalue cutoff of 10. Simulated DAS-beamformed images of MB flow channel in (C) free field, (D) through NHP and (E) human skulls. Center of the flow channel in free field and after skull transmission indicated by white asterisk and cyan circle, respectively.

the flow channel through the NHP skull of 0.50 mm and 0.13 mm, respectively (Fig. 3D), and axial and lateral shifts through the human skull of 1.13 mm and 0.50 mm, respectively (Fig. 3E). While there was an average discrepancy in axial and lateral shifts of 0.54 mm and 0.49 mm, respectively for both skull models when compared to PCI, simulated flow channel position agreed well with in vitro transcranial PCI within 3.0 – 8.6 percent error.

IV. Discussion and Conclusions

This study demonstrates the feasibility of performing transcranial passive cavitation imaging through primate skull models in a single, theranostic phased array system. Predicted focal shifts after transcranial transmission through both skull models confirmed by in vitro hydrophone experiments agreed well with simulated results. Average axial and lateral focal shifts upon transcranial transmission through the skull of approximately 2 mm and 1 mm, respectively, demonstrate the feasibility of using the P4-1 phased array for accurate targeting through primate skulls. Furthermore, shifts in the apparent location of a channel containing flowing microbubbles maintained within the physiological flow velocity for cerebral capillaries and small arterioles of 0.5-3.0 mm/s [9], imaged by transcranial PCI indicated minimal registration errors, suggesting that PCI may be an accurate technique for transcranial mapping of cavitation activity in a cerebral vessel. These registration errors imaged by PCI also agreed well with both simulated results, and the results of other studies using the P4-1 for transcranial super-resolution imaging at 2.5 MHz [10]. Future work includes assessing BBB opening and monitoring capability through primate skulls in vivo, further characterizing the effects of skull geometry on the focal distortion of the P4-1 diagnostic phased array, and implementing PCI post-processing techniques such as phase aberration correction and dynamic SVD clutter filter eigenvalue cutoff selection for transcranial PCI.

In summary, this work provides an initial feasibility study for transcranial power cavitation imaging used to monitor BBB opening through primate skulls.

Acknowledgements

The authors wish to thank UEIL members Robin Ji, Mark Burgess, Antonios Pouliopoulos and Omid Yousefian.

References

[1] H. Chen and E. E. Konofagou, "The size of blood-brain barrier opening induced by focused ultrasound is dictated by the acoustic pressure," *J. Cereb. Blood Flow Metab. Off. J. Int. Soc. Cereb. Blood Flow Metab.*, vol. 34, no. 7, pp. 1197–1204, Jul. 2014, doi: 10.1038/jcbfm.2014.71.

[2] T. Sun, G. Samiotaki, S. Wang, C. Acosta, C. C. Chen, and E. E. Konofagou, "Acoustic cavitation-based monitoring of the reversibility and permeability of ultrasound-induced blood-brain barrier opening," *Phys. Med. Biol.*, vol. 60, no. 23, pp. 9079–9094, Dec. 2015, doi: 10.1088/0031-9155/60/23/9079.

[3] Y.-S. Tung, F. Vlachos, J. J. Choi, T. Deffieux, K. Selert, and E. E. Konofagou, "In vivo transcranial cavitation threshold detection during ultrasound-induced blood–brain barrier opening in mice," *Phys. Med. Biol.*, vol. 55, no. 20, pp. 6141–6155, Oct. 2010, doi: 10.1088/0031-9155/55/20/007.

[4] S.-Y. Wu *et al.*, "Transcranial Cavitation Detection in Primates during Blood-Brain Barrier Opening – A Performance Assessment Study," *IEEE Trans. Ultrason. Ferroelectr. Freq. Control*, vol. 61, no. 6, pp. 966–978, Jun. 2014, doi: 10.1109/TUFFC.2014.2992.

[5] M. Gyongy and C.-C. Coussios, "Passive Spatial Mapping of Inertial Cavitation During HIFU Exposure," *IEEE Trans. Biomed. Eng.*, vol. 57, no. 1, pp. 48–56, Jan. 2010, doi: 10.1109/TBME.2009.2026907.

[6] C. D. Arvanitis, C. Crake, N. McDannold, and G. T. Clement, "Passive Acoustic Mapping with the Angular Spectrum Method," *IEEE Trans. Med. Imaging*, vol. 36, no. 4, pp. 983–993, Apr. 2017, doi: 10.1109/TMI.2016.2643565.

[7] P. J. White, G. T. Clement, and K. Hynynen, "Local frequency dependence in transcranial ultrasound transmission," *Phys. Med. Biol.*, vol. 51, no. 9, pp. 2293–2305, May 2006, doi: 10.1088/0031-9155/51/9/013.

[8] M. T. Burgess, I. Apostolakis, and E. E. Konofagou, "Power cavitation-guided blood-brain barrier opening with focused ultrasound and microbubbles," *Phys. Med. Biol.*, vol. 63, no. 6, p. 065009, Mar. 2018, doi: 10.1088/1361-6560/aab05c.

[9] K. P. Ivanov, M. K. Kalinina, and Yu. I. Levkovich, "Blood flow velocity in capillaries of brain and muscles and its physiological significance," *Microvasc. Res.*, vol. 22, no. 2, pp. 143–155, Sep. 1981, doi: 10.1016/0026-2862(81)90084-4.

[10] D. E. Soulioti, D. Espíndola, P. A. Dayton, and G. Pinton, "Super-resolution imaging through the human skull," *IEEE Trans. Ultrason. Ferroelectr. Freq. Control*, pp. 1–1, 2019, doi: 10.1109/TUFFC.2019.2937733.